Catalysis Today 165 (2011) 120–128

Contents lists available at ScienceDirect

Catalysis Today

journal homepage: www.elsevier.com/locate/cattod

Reaction mechanism of tert-butylation of phenol with tert-butyl alcohol over H-β zeolite: An ONIOM study

Xiaowa Nie[a,c], Michael J. Janik[b], Xinwen Guo[a,*], Xin Liu[a], Chunshan Song[a,b,c,**]

[a] State Key Laboratory of Fine Chemicals, School of Chemical Engineering, Dalian University of Technology, Dalian 116012, China
[b] Department of Chemical Engineering, Pennsylvania State University, University Park, PA 16802, USA
[c] EMS Energy Institute and Department of Energy & Mineral Engineering, Pennsylvania State University, University Park, PA 16802, USA

ARTICLE INFO

Article history:
Available online 6 January 2011

Keywords:
Phenol
Tert-butylation
H-β
Zeolite
Reaction mechanism
ONIOM

ABSTRACT

Tert-butylation of phenol with tert-butyl alcohol (TBA) over H-β zeolite was studied using the ONIOM approach with two proposed reaction paths: stepwise and concerted mechanisms. The results obtained by the ONIOM2 (B3LYP/6-31G(d,p):UFF) method reveals that the tert-butylation of phenol preferentially occurs through a co-adsorbed, concerted mechanism without prior dehydration of tert-butyl alcohol, rather than via a stepwise mechanism through dehydration to form tert-butyl carbenium ion as the first step followed by tert-butyl cation attack on the 2- or 4-position on phenol. The kinetic difference between 2- and 4-tert-butylation is more apparent in the concerted path, where 4-tert-butylation proceeds over a lower activation barrier. Decreasing the acid site strength, via substitution of Ga for Al, reduces the H-bonding interaction between the zeolitic proton and tert-butyl alcohol and increases the apparent activation barriers, which slows the overall reaction, and also lowers the selectivity to 4-tert-butyl phenol.

1. Introduction

Zeolites, as eco-benign solid catalysts, are widely used in petrochemical processes due to their high activity and selectivity [1–8]. Tert-butylation of phenol with tert-butyl alcohol (TBA) over zeolites has been extensively investigated owing to the industrial interest in the production of 4-tert-butyl phenol as an antioxidant, ultraviolet adsorber and heat stabilizer of polymeric materials [9–11]. H-β zeolite has potential as an effective catalyst for this reaction by virtue of its high silica content and suitable acid site distribution [9,12]. Tert-butylation of phenol with TBA over zeolites includes two competitive reactions to produce the mono-C-tert-butylation products—2-tert-butyl phenol (2-TBP) and 4-tert-butyl phenol (4-TBP), respectively. High selectivity to 4-TBP is desired because this product imparts improved performance to metallic detergents (phenates) used in lubricating oils [13], and can be used in the manufacture of phenolic resins, antioxidants, polymerization inhibitors, lube additives, and substituted triaryl phosphates [10]. With zeolites as the acidic catalysts, 4-TBP is produced as the dominant product.

The choice of an optimal solid acid catalyst for tert-butylation requires relating the acid site structure, acidity, and strength to the activity and selectivity for the given reaction. The acidity is defined by the number of acid sites in a unit weight or unit surface area, and for a specific zeolite structure, it is dictated by the Si:Al or Si:Ga ratio. A number of experimental measures may be used to characterize the acid strength of a solid acid, including the Hammett acidity function (H_0), adsorption of basic probe molecules, and ^{1}H nuclear magnetic resonance. These measures can differ in their ranking of acid strength. Computationally, the proton affinity of a conjugate base site can be used to rank acid strength.

A number of experimental studies have related the zeolite activity and selectivity for tert-butylation of phenol to acid properties. Zhang et al. [9] reported that, for tert-butylation of phenol with TBA over H-β zeolite, medium strength acid sites are advantageous in producing 4-TBP, whereas weak acid sites are effective in producing 2-TBP. Sakthivel et al. [10] carried out the para-selective tert-butylation of phenol with TBA over mesoporous H-AlMCM-41, and found that H-AlMCM-41 with moderate acidity is advantageous for 4-TBP formation. Song et al. [11] studied the alkylation of phenol with TBA catalyzed by a mesoporous material with enhanced acidity synthesized from zeolite MCM-22, and demonstrated weak acid sites mainly produce 2-TBP, moderate acid sites give 4-TBP, and strong acid sites enhance the selectivity to 2,4-di-tert-butyl phenol (2,4-DTBP). Despite these experimental kinetic studies, the

* Corresponding author at: Dalian University of Technology, PO Box 39, No. 158 Zhongshan Rd, Dalian 116012, China.
Tel.: +86 411 39893990; fax: +86 411 39893991.
** Corresponding author at: EMS Energy Institute and Department of Energy & Mineral Engineering, Pennsylvania State University, University Park, PA 16802, USA.
Tel.: +1 814 863 4466; fax: +1 814 865-3573.
E-mail addresses: guoxw@dlut.edu.cn (X. Guo), csong@psu.edu (C. Song).

0920-5861/$ – see front matter © 2010 Elsevier B.V. All rights reserved.
doi:10.1016/j.cattod.2010.11.070

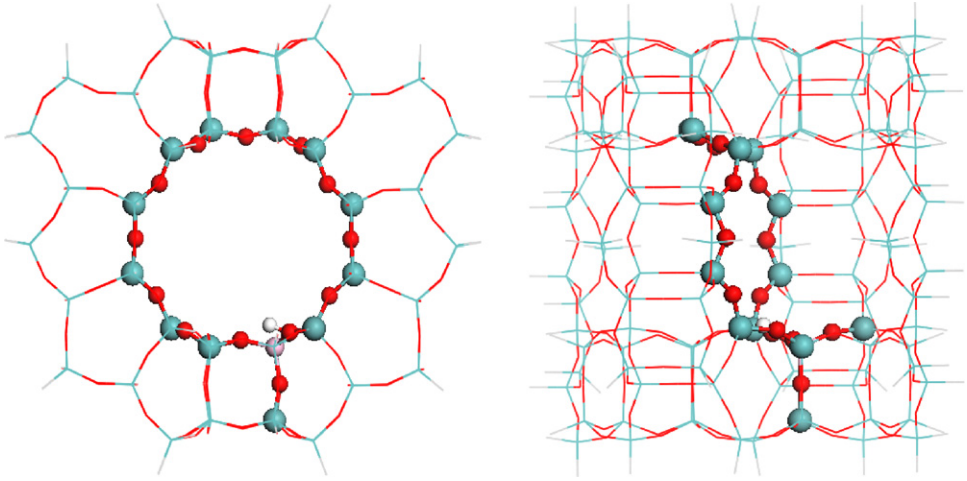

Fig. 1. 116T cluster model of H-Al-β zeolite subdivided into two layers according to the two-layer ONIOM (ONIOM2) approach: the inner 14T cluster (balls) was computed with the B3LYP/6-31G(d,p) level of theory, and the remainder (lines) was treated with the universal force field (UFF) method (blue: silicon, red: oxygen, pink: aluminum, white: hydrogen). (For interpretation of the references to color in this figure legend, the reader is referred to the web version of the article.)

reaction mechanism for tert-butylation of phenol with TBA over solid acid catalysts remains unclear. Without knowledge of how the intermediate or transition state interacts with the active site, determination of optional acid properties of a zeolite catalyst for this reaction remains empirical.

Theoretical calculations based on quantum chemistry are a helpful tool to investigate the reaction mechanism at a molecular level. Small clusters are often adapted as models of zeolite reaction sites, however, these models do not include the framework influence, which may play an important role for reactions in zeolite pores [14–16]. The "own-*N*-layered integrated molecular orbital + molecular mechanics" (ONIOM) method combines different theoretical levels of calculation to investigate adsorption and reaction of hydrocarbons over zeolites [17–21]. The active site and inner-pore surface are considered using density functional theory and the extended framework is represented with molecular mechanics. In this work, the ONIOM approach is used to determine the reaction mechanism of tert-butylation of phenol in the H-β zeolite pore, and to study the influence of H-β acid site strength on this reaction.

2. Models and methods

The acidic H-β zeolite was represented by the 116T cluster model taken from the lattice structure of beta zeolite [22–25], as shown in Fig. 1. The cluster was terminated by H atoms bonded to Si atoms, with the terminal Si–H bond length fixed at 1.47 Å. We first used a single Al atom substituted for Si1 (T1) to introduce an acid site [25], then substituted Ga for Al to alter the acid site strength. A two layer ONIOM (ONIOM2) approach was employed for computational efficiency. Within this method, density functional theory based calculation at the B3LYP/6-31G(d,p) level was applied to the inner 14T cluster, covering the 12-membered ring and two additional basal T units. This was considered to represent the active region of the β-zeolite. The remaining extended zeolite framework was treated with the universal force field (UFF) [26]. During optimization, only the basic 5T cluster of the 14T active region, [(≡(SiO)$_3$Al(OH)Si≡] or [(≡(SiO)$_3$Ga(OH)Si≡], was allowed to relax, whereas the rest of the model was fixed at the crystallographic coordinates. The QST method within the framework of DFT was used to isolate transition states, and each transition state was confirmed to have a single imaginary vibrational frequency along the reaction coordinate. Zero-point energy (ZPE) corrections were included. All calculations were conducted with the Gaussian 03 package [27].

We calculated the proton affinity (PA) of zeolites and adsorption energy of an NH_3 molecule to characterize the acid site strength of the Al and Ga substituted beta zeolites. The PA is calculated as:

$$PA = E_{(ZeOH)} - E_{(ZeO^-)} - E_{(H^+)}, \quad (1)$$

where $E_{(ZeOH)}$ is the total energy of the zeolite cluster ZeOH, $E_{(ZeO^-)}$ is the total energy of the corresponding anion, and $E_{(H^+)}$ is the total energy of a proton (defined as zero in Gaussion 03). The adsorption energy of NH_3 was referred to that of the isolated NH_3 molecule in gaseous phase and the zeolite system:

$$\Delta E_{(ads)} = E_{(NH_3\text{-zeolote})} - E_{(NH_3)} - E_{(zeolite)} \quad (2)$$

3. Results and discussion

We proposed two reaction paths for tert-butylation of phenol with TBA over H-β, based on relevant studies regarding acid-catalyzed alkylation reactions [19,28,29]: the stepwise and the concerted mechanisms, as shown in Scheme 1(a) and (b), respectively. ONIOM results for the reaction path of each mechanism are presented in Sections 3.1 (stepwise) and 3.2 (concerted) followed by a comparison of the two mechanisms (Section 3.3) and examination of the impact of Ga substitution on energetics (Section 3.4). The Cartesian coordinates for all stationary points included, as well as the imaginary frequency values for each transition state created in both the reaction mechanisms with Al-H-β and Ga-H-β are given in Supplementary Data.

3.1. Stepwise mechanism

3.1.1. Formation of the tert-butyl carbenium ion

In the stepwise mechanism, we first examined the TBA dehydration. A TBA molecule adsorbs at the active site of acidic H-β zeolite through formation of an $O_{alcohol}$–$H_{zeolite}$ hydrogen bond. The TBA C–O bond is then cleaved to generate a tert-butyl carbenium ion product, releasing a water molecule. This dehydration step produces a tert-butyl carbenium ion that can either deprotonate to form isobutene, or react with co-adsorbed phenol, to form the tert-butylation product.

The stepwise path occurs through the creation of a tert-butyl carbenium ion product in the first step. In relevant studies on alcohol dehydration over acidic zeolites, an alkoxide state is found after alcohol dehydration, with the central carbon atom ($C_{alcohol}$) of the

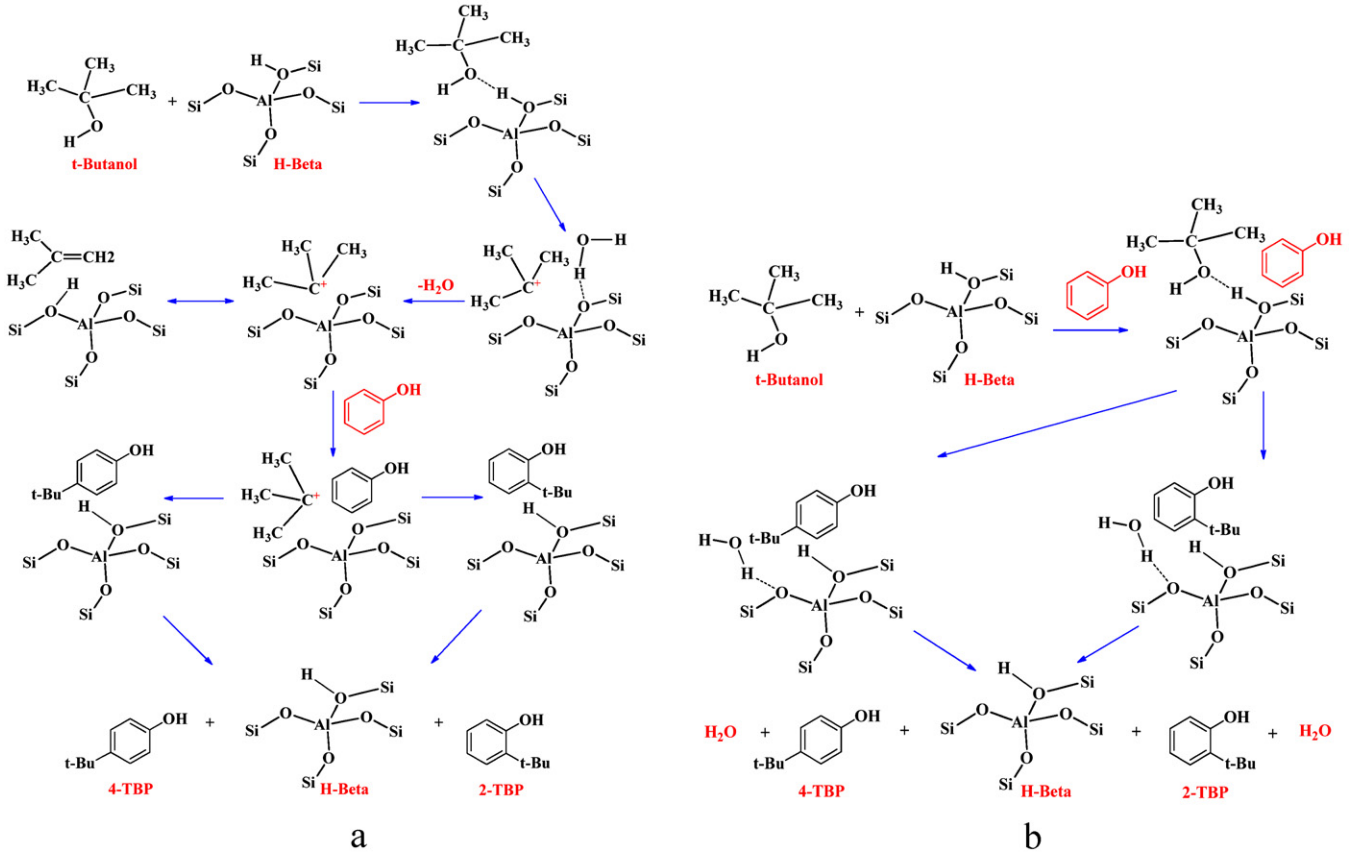

Scheme 1. Proposed reaction paths for tert-butylation of phenol with TBA over H-β, (a) the stepwise mechanism and (b) the concerted mechanism.

alkyl carbenium ion bonded with the negatively charged basic site ($O_{zeolite}$) of the zeolite [18,28–33]. Therefore, we first tried to construct a tert-butyl alkoxide state inside the H-β pore. However, after geometric optimization, the $C_{alcohol}$–$O_{zeolite}$ bond dissociated to form a tert-butyl carbenium ion interacting with the negatively charged basic site. Rotation of the initial tert-butyl alkoxide structure did not allow for the $C_{alcohol}$–$O_{zeolite}$ bond to be stabilized. The difference in TBA dehydration product structure compared to other alcohols (such as methanol, ethanol and propanol) may result from the larger repulsive van der Waals (vdW) interaction between the bulky tert-butyl group and the zeolite framework.

The optimized geometric parameters of the adsorbed TBA, the dehydration transition state, and the tert-butyl carbenium ion product are given in Table 1. In the structures of these three molecules, O_1 represents the conjugated base site of the original acid site for H-β zeolite, O_2 is for interacting with tert-butyl carbenium ion, and O_3 belongs to the hydroxyl group of TBA molecule. The adsorption geometry of TBA, **Ads_*t*-Bu**, is shown in Fig. 2(a). The initial O_1–H_1 bond of H-β zeolite is lengthened from 0.97 Å prior to TBA adsorption to 1.09 Å and the interatomic distance between O_3 and H_1 is 1.39 Å, which indicates a hydrogen bond is formed between the TBA hydroxyl group and the acid site of the zeolite framework. In the adsorption structure of TBA, the C_1–O_3 bond is elongated from 1.43 Å in the isolated state to 1.48 Å due to interaction with the Brønsted acid site. The TBA C–O bond is therefore activated toward cleavage.

Table 1
Geometric parameters of all species involved in tert-butyl carbenium ion formation in the stepwise mechanism over Al-H-β[a] (atom labels are given in Fig. 2).

Parameter	Ads_*t*-Bu	TS_Car	Int_Car. . .H_2O
Distances			
C_1–O_3	1.48	3.22	3.50
O_3–H_1	1.39	0.97	0.98
H_1–O_1	1.09	2.12	2.05
Si–O_1	1.64	1.57	1.58
Al–O_1	1.77	1.68	1.68
Si–O_2	1.59	1.58	1.58
Al–O_2	1.67	1.69	1.69
Angles			
Si–O_1–Al	135.2	139.1	137.2
Si–O_2–Al	131.0	132.8	133.7

[a] Distances are in Angstroms, angles are in degrees.

The transition state, **TS_Car**, for formation of the carbenium ion product is shown in Fig. 2(b). The C_1–O_3 bond is broken at the transition state, as demonstrated by its elongation from 1.48 Å in the adsorbed state to 3.22 Å. The atomic distance between O_3 and H_1 is 0.97 Å, which is similar to the O–H bond length (0.96–0.98 Å) of water, indicating a water molecule is formed at the transition state. The geometry about the C_1 atom of the tert-butyl group changes from tetrahedral in adsorbed TBA to trigonal planar, owing to the C_1 hybridization state change from sp^3 to sp^2.

The adsorbed tert-butyl carbenium ion product (**Int_Car. . .H_2O**) is shown in Fig. 2(c). The C_1 substituents of the tert-butyl carbenium ion are co-planer with the C_1 atom, indicating the hybridization state of the C_1 atom is sp^2. The structure within the acid site, carbenium ion, and water molecule are similar between the dehydration transition state and product, however, they show differences in relative location. At the transition state, the tert-butyl carbenium ion has a further distance between the central carbon atom and the framework O atom of zeolite (C_1–O_2 is 4.26 Å), but a nearer distance with the O atom of water (C_1–O_3 is 3.22 Å). At the product state, the tert-butyl carbenium ion moves further from the O atom of water (C_1–O_3 is 3.50 Å) and closer to the O atom of the zeolite framework (C_1–O_2 is 3.56 Å).

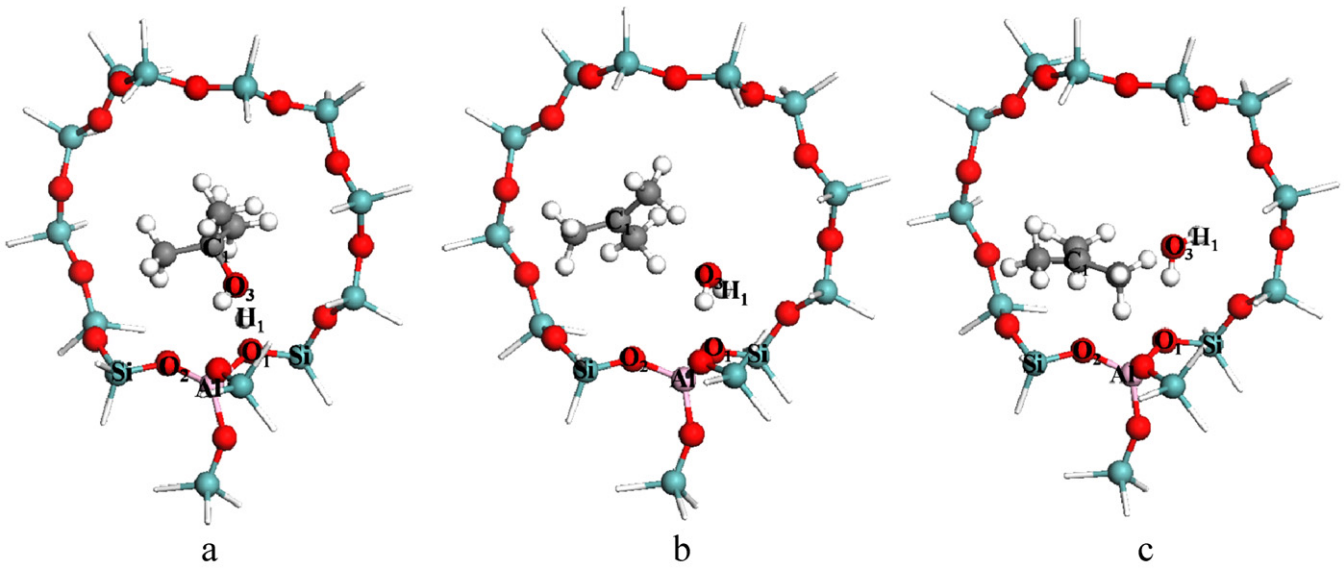

Fig. 2. Optimized geometries of (a) TBA adsorption, Ads_*t*-Bu; (b) the transition state for tert-butyl carbenium ion product formation, TS_Car; (c) the tert-butyl carbenium ion, Int_Car. . .H_2O. (Only the active region of the Al-H-β zeolite is shown for clarity) (blue: silicon, red: oxygen, pink: aluminum, white: hydrogen). (For interpretation of the references to color in this figure legend, the reader is referred to the web version of the article.)

The relative energy of all species involved in formation of the carbenium ion product is depicted in Fig. 3. The energy of separated TBA plus the zeolite cluster is used as the reference point. The adsorption energy of TBA is −30.0 kcal mol^{-1}, which is more exothermic compared with the experimental estimation of the methanol adsorption enthalpy in acidic H-ZSM-5 zeolite, ranging from −15 to −27 kcal mol^{-1} [34,35]. The more exothermic adsorption energy of TBA over H-β zeolite likely results from the attractive vdW interaction with zeolite pore for the bigger TBA molecule and the stronger acidity of H-β than H-ZSM-5 [36]. The activation energy barrier (E_{act}) for **Int_Car**. . .**H_2O** formation is 30.6 kcal mol^{-1}, which is 9.0 and 9.9 kcal mol^{-1} lower than that for methoxide formation over H-FAU [29] and ethoxide formation over H-ZSM-5 [28]. The formation of the tert-butyl carbenium ion product is endothermic relative to the adsorbed TBA state by 27.4 kcal mol^{-1}.

Once the tert-butyl carbenium ion is generated, the water molecule may be released from the pore. We did not consider the impact of adsorbed water on the subsequent alkylation reactions, and this assumption is discussed further in comparing the stepwise and concerted mechanisms (Section 3.3). We therefore define the "stepwise mechanism" to require water desorption prior to tert-butylation. The desorption energy of water is 12.7 kcal mol^{-1}. The carbenium ion **(Int_Car)** could further deprotonate to form isobutene or react with phenol. Isobutene is produced by deprotonation of the carbenium ion, and it must be reactivated by a Brønsted acid site to recreate the tert-butyl carbenium ion for tert-butylation to occur. The E_{act} for formation of **Int_Car** from isobutene is 9.5 kcal mol^{-1}, whereas the E_{act} for formation of isobutene is 2.1 kcal mol^{-1}. This implies that interchange between isobutene and the carbenium ion is facile even under moderate temperature, and this reaction can be considered equilibrated within the overall tert-butylation reaction scheme.

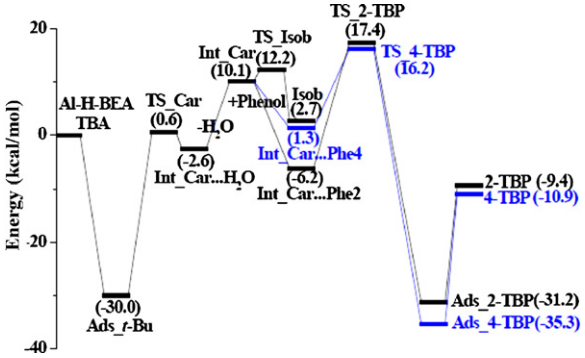

Fig. 3. Relative energy (kcal mol^{-1}) of all species involved in the stepwise mechanism of phenol tert-butylation with TBA over Al-H-β. (The energy of separated TBA plus Al-H-β is used as the reference point).

3.1.2. *Tert-butylation of phenol*

To initiate the tert-butylation sequence, a phenol molecule is co-adsorbed in the zeolite pore with the carbenium ion. The important geometric parameters of the co-adsorbed species, transition states, and product states for 2- and 4-tert-butylation in the stepwise mechanism are given in Table 2. In 2-tert-butylation, the optimized co-adsorbed phenol with the tert-butyl carbenium ion is shown in Fig. 4(a) and labeled **Ads_Car**. . .**Phe2**. The distance between the H atom of the hydroxyl of phenol and the zeolite framework O atom is 2.54 Å, indicating possible weak hydrogen bond interaction between these two atoms. The atomic distance between C_1–C_2 and C_2–O_2 is 4.70 and 3.18 Å, respectively. Phenol is largely stabilized by the tert-butyl carbenium ion through partial positive-negative charge interaction between the carbenium ion and the π electrons in the benzene ring of phenol. Therefore, the positive charge in the carbenium ion may be stabilized by both the negatively charged basic site of the zeolite and the π electrons in the benzene ring of phenol. For 4-tert-butylation, the co-adsorbed phenol with the carbenium ion is shown in Fig. 4(b), **Ads_Car**. . .**Phe4.** The C_1–C_2 and C_2–O_2 atomic distance is 4.48 and 3.20 Å, respectively. The co-adsorption energy of phenol with the carbenium ion is −16.3 and −8.8 kcal mol^{-1} for 2- and 4-tert-butylation, as shown in Fig. 3. This difference in co-adsorption stability results from difference in the hydrogen bond interaction involving in the **Ads_Car**. . .**Phe2**. The co-adsorption of phenol with the carbenium ion is exothermic and therefore these two species can co-locate inside the zeolite pore.

The formation of the transition state, **TS_2-TBP**, as shown in Fig. 4(c), involves the concerted action of formation of a C_1-C_2 bond and cleavage of the C_1-H_1 bond. Similar bond cleavage and formation occur at the transition state in 4-tert-butylation,

Table 2
Important bond parameters of all species involved in the tert-butylation step within the stepwise mechanism over Al-H-β[a] (atom labels are given in Fig. 4).

Parameter	Ads_Car. . .Phe2	Ads_Car. . .Phe4	2-Tert-butylation		4-Tert-butylation	
			TS_2-TBP	Ads_2-TBP	TS_4-TBP	Ads_4-TBP
Distances						
C_1–C_2	4.70	4.48	1.59	1.54	1.59	1.54
C_1–H_1	1.09	1.10	1.36	3.14	1.35	3.07
H_1–O_1	3.78	2.43	1.65	0.98	1.61	0.98
Si–O_1	1.57	1.57	1.65	1.66	1.66	1.66
Al–O_1	1.66	1.66	1.78	1.81	1.80	1.81
Si–O_2	1.57	1.57	1.59	1.60	1.59	1.60
Al–O_2	1.69	1.69	1.67	1.67	1.67	1.67
Angles						
C_2–C_1–H_1	42.0	56.6	110.7	102.2	110.3	96.9
C_1–H_1–O_1	124.3	154.6	173.7	155.1	174.0	156.6
Si–O_1–Al	140.0	140.0	127.9	136.5	133.5	136.6
Si–O_2–Al	134.2	134.2	131.3	128.3	129.9	128.4

[a] Distances are in Angstroms, angles are in degrees.

TS_4-TBP, as shown in Fig. 4(d). The vibrational animation of the single imaginary frequency for these two transition states shows both C_1–C_2 formation and the hydrogen transfer from the carbon atom of phenol to the negatively charged basic site of the zeolite. The activation barriers are 23.6 and 14.9 kcal mol^{-1} for 2- and 4-tert-butylation from the co-adsorbed states. The 8.7 kcal mol^{-1} difference indicates that formation of 4-TBP is kinetically more favored than 2-TBP formation. As the proton is back-donated to regenerate the acid site of the zeolite during tert-butylation, the final step is product desorption from the active site of the zeolite. Fig. 3 shows that formation of adsorbed 2-TBP from the co-adsorbed state is exothermic by 25.0 kcal mol^{-1}, whereas it is 36.6 kcal mol^{-1} exothermic for adsorbed 4-TBP formation. The overall reaction energy is −9.4 kcal mol^{-1} exothermic for 2-TBP formation and −10.9 kcal mol^{-1} exothermic for 4-TBP formation. The more exothermic reaction energy for 4-TBP formation indicates that 4-TBP is the thermodynamically more stable product.

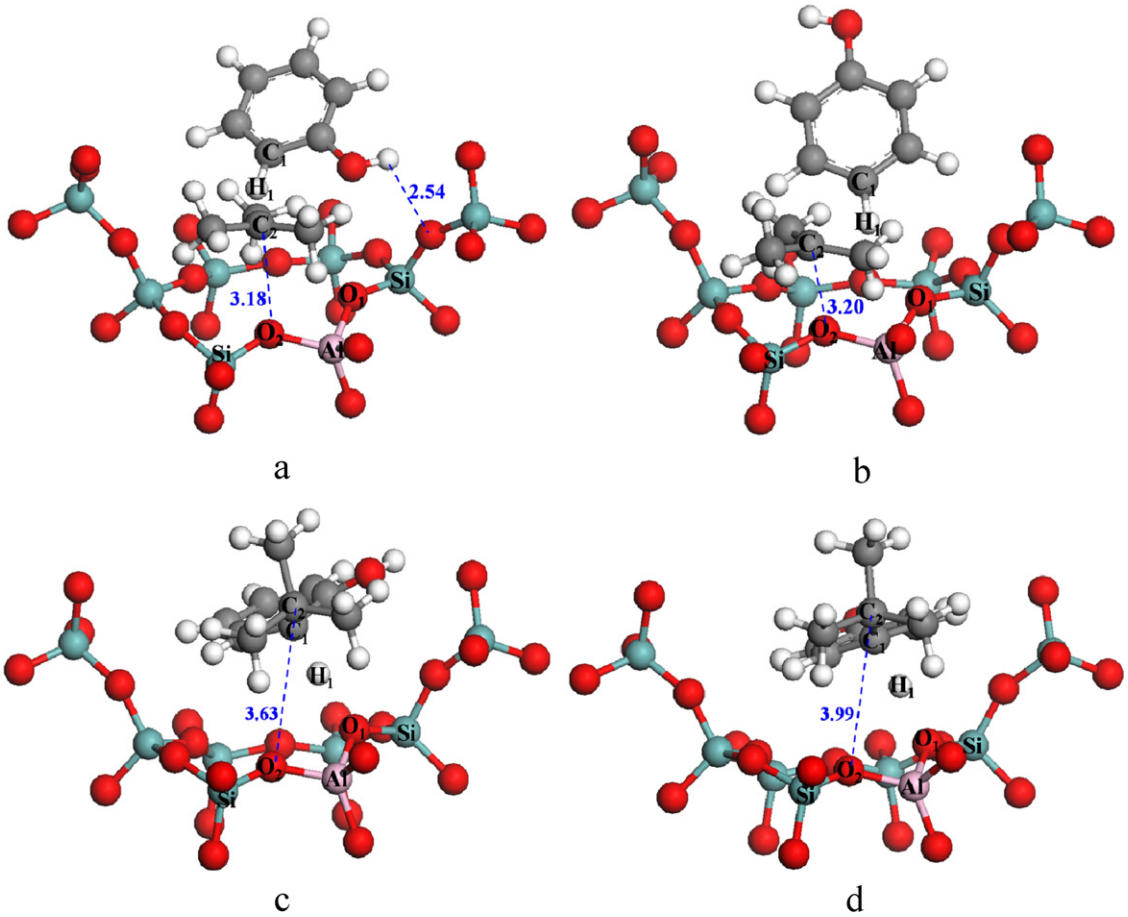

Fig. 4. Optimized geometries of the co-adsorbed states and tert-butylation transition states in the stepwise mechanism. Co-adsorbed states are shown in (a) 2-tert-butylation, Ads_Car. . .Phe2 and (b) 4-tert-butylation, Ads_Car. . .Phe4; transition states are shown in (c) 2-tert-butylation, TS_2-TBP and (d) 4-tert-butylation, TS_4-TBP (Al-H-β zeolite structure is shown in part for clarity) (blue: silicon, red: oxygen, pink: aluminum, white: hydrogen). (For interpretation of the references to color in this figure legend, the reader is referred to the web version of the article.)

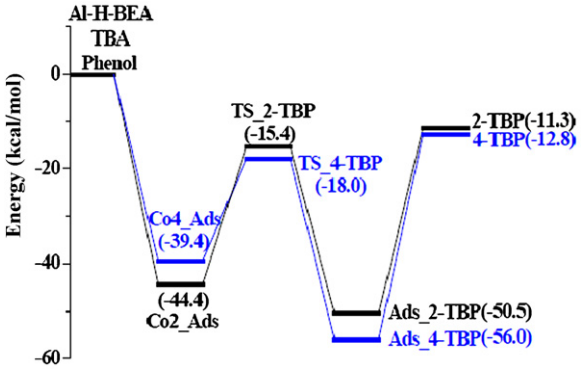

Fig. 5. Relative energy (kcal mol^{-1}) for each state in the concerted mechanism of phenol tert-butylation with TBA over Al-H-β. (The energy of separated TBA, Al-H-β plus separated phenol is used as the reference point.)

3.2. Concerted mechanism

The concerted tert-butylation mechanism occurs with initial co-adsorption of phenol and TBA, followed by the tert-butylation of phenol with TBA directly without formation of a tert-butyl carbenium ion. The relative stability for each state of this path is shown in Fig. 5, reactant and transition state structures are illustrated in Fig. 6, and the optimized structural parameters of species involved are given in Table 3. In the molecular structures, O_1 represents the conjugated base site of the original acid site for H-β zeolite, O_2 is for proton donation after tert-butylation reaction, and O_3 belongs to the hydroxyl group of TBA molecule.

To construct an initial co-adsorbed configuration, the adsorption of TBA and phenol were first separately optimized. For phenol, there are two kinds of adsorption models including that via hydrogen bond interaction between the –OH group of phenol and the acid site of H-β zeolite, and that via π–H bond interaction between the benzene ring of phenol and the acid site of H-β zeolite, as shown in Supplementary Data. By comparison of the adsorption energies of these two adsorption structures, phenol adsorbs through a hydrogen bond interaction is thermodynamically more stable, with an adsorption energy of −19.3 kcal mol^{-1}, which is slightly lower than the DFT result (−22.3 kcal mol^{-1}) by Sasaki et al. [37] using the Re_4O_{10} cluster of H-ZSM-5. The adsorption energy of TBA over H-β zeolite is −30.0 kcal mol^{-1}, which is comparable with the computational results on silicalite (27.3 kcal mol^{-1}) and H-ZSM-5 (30.8 kcal mol^{-1}) by Shubin et al. [38], thus TBA adsorption is preferred thermodynamically over phenol adsorption. TBA is adsorbed over the acid site of H-β zeolite via a hydrogen bond interaction, and the phenol molecule is co-adsorbed nearby. These structures are labeled **Co2_Ads** for 2-tert-butylation and **Co4_Ads** for 4-tert-butylation, as shown in Fig. 6(a) and (b). In **Co2_Ads**, the H atom of the hydroxyl group of phenol has a hydrogen bond interaction with a framework O atom of the zeolite with a H_{phenol}–$O_{zeolite}$ distance of 2.54 Å. The tert-butyl group of TBA has partially delocalized positive charge because the negative charge on the hydroxyl O atom

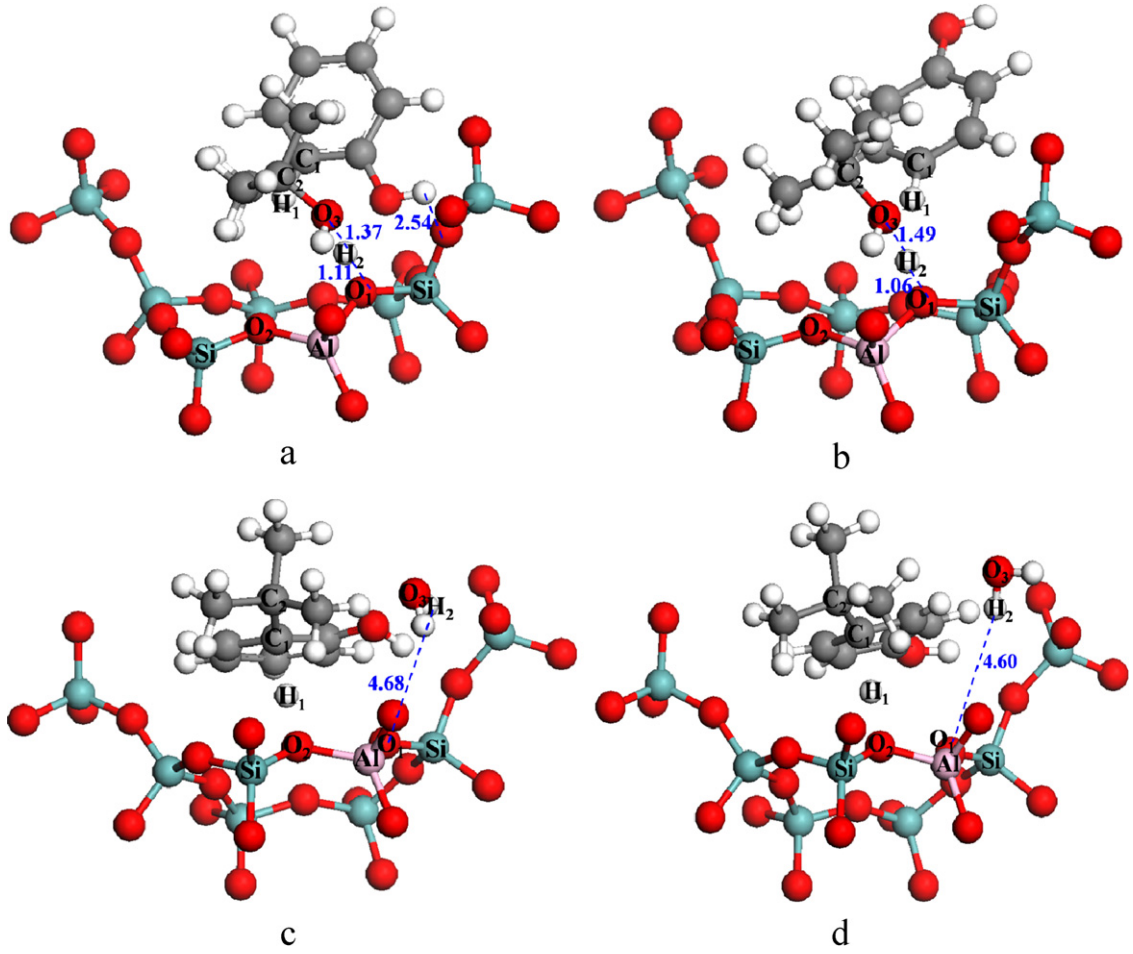

Fig. 6. Optimized geometries of the co-adsorbed reactants and transition states in the concerted mechanism. Co-adsorbed reactants are shown in (a) 2-tert-butylation, Co2_Ads and (b) 4-tert-butylation, Co4_Ads; transition states are shown in (c) 2-tert-butylation, TS_2-TBP and (d) 4-tert-butylation, TS_4-TBP. (Al-H-β zeolite structure is shown in part for clarity) (blue: silicon, red: oxygen, pink: aluminum, white: hydrogen). (For interpretation of the references to color in this figure legend, the reader is referred to the web version of the article.)

Table 3
Optimized structural parameters for each state involved in 2- and 4-tert-butylation in the concerted mechanism over Al-H-β[a] (atom labels are given in Fig. 6).

Parameter	Co2_Ads	Co4_Ads	2-Tert-butylation		4-Tert-butylation	
			TS_2-TBP	Ads_2-TBP	TS_4-TBP	Ads_4-TBP
Distances						
C_2–O_3	1.48	1.48	4.10	4.09	4.15	4.12
C_1–C_2	4.72	4.69	1.59	1.54	1.57	1.54
C_1–H_1	1.09	1.09	1.46	3.25	1.47	3.15
O_2–H_1	3.99	3.87	1.36	0.98	1.36	0.98
Si–O_1	1.63	1.65	1.56	1.58	1.56	1.58
Al–O_1	1.77	1.78	1.67	1.66	1.66	1.65
Si–O_2	1.59	1.59	1.65	1.68	1.63	1.68
Al–O_2	1.67	1.66	1.76	1.81	1.75	1.81
Angles						
C_2–C_1–H_1	75.1	49.4	108.8	102.2	115.6	102.8
C_1–H_1–O_2	136.3	158.3	176.6	146.8	177.8	147.1
Si–O_1–Al	134.1	134.1	140.5	134.4	140.3	135.2
Si–O_2–Al	131.1	131.1	124.9	131.1	126.6	131.4

[a] Distances are in Angstroms, angles are in degrees.

transfers in part to the H acid site of the zeolite. The partially delocalized positive charge on tert-butyl group of TBA appears to be stabilized by the π electrons in the benzene ring of phenol for both the **Co2_Ads** and **Co4_Ads**.

After the co-adsorption, phenol is attacked by TBA directly, leading to the formation of 2-TBP or 4-TBP and releasing a water molecule. The concerted reaction breaks the $O_{zeolite}$–$H_{zeolite}$ bond, forms the $O_{alcohol}$–$H_{zeolite}$ bond, breaks the $C_{alcohol}$–$O_{alcohol}$ bond, forms the $C_{alcohol}$–C_{phenol} bond, breaks the C_{phenol}–H_{phenol} bond and forms the H_{phenol}–$O_{zeolite}$ bond in a single step. The transition states for 2-tert-butylation, **TS_2-TBP** and 4-tert-butylation, **TS_4-TBP** in the concerted path are shown in Fig. 6(c) and (d), respectively. At the transition state, the $O_{zeolite}$–$H_{zeolite}$ bond is broken, with the $O_{zeolite}$–$H_{zeolite}$ (O_1–H_2) distance of 4.68 Å for **TS_2-TBP** and 4.60 Å for **TS_4-TBP**. The $O_{alcohol}$–$H_{zeolite}$ (O_3–H_2) bond is formed and the $C_{alcohol}$–$O_{alcohol}$ (C_2–O_3) bond is completely broken to produce a water molecule for both transition states. The other H atom in water interacts with a framework O atom of the zeolite, which is not shown in the figure for clarity. The $C_{alcohol}$–C_{phenol} (C_2–C_1) bond is partially formed, with the $C_{alcohol}$–C_{phenol} bond length of 1.59 Å for **TS_2-TBP** and 1.57 Å for **TS_4-TBP**, which are 0.05 and 0.03 Å longer than the $C_{alcohol}$–C_{phenol} bond length (1.54 Å) in the adsorbed products. The C_{phenol}–H_{phenol} (C_1–H_1) bond is elongated at the transition state, but the H_{phenol}–$O_{zeolite}$ (H_1–O_2) bond is incompletely formed. The atomic distance between the C_{phenol} and H_{phenol} is 1.46 Å for **TS_2-TBP** and 1.47 Å for **TS_4-TBP**, which are much longer than the original C_{phenol}–H_{phenol} bond length (1.09 Å) in the co-adsorbed reactants. However, the H_{phenol}–$O_{zeolite}$ bond distance (1.36 Å for both transition states) is too far to form a H–O bond completely, as compared with the H–O bond length (0.96–0.99 Å) of the acid site of H-β. Though the transition state is for the "concerted" path, the transition state structure indicates that proton transfer from phenol to the zeolite occurs as the $C_{alcohol}$–C_{phenol} bond is formed whereas the alcohol dehydration portion is already completed.

The co-adsorption energies of **Co2_Ads** and **Co4_Ads** are −44.4 and −39.4 kcal mol^{-1}. This 5.0 kcal mol^{-1} difference in adsorption energy mainly results from the difference in adsorption structure of the phenol molecule. In 2-tert-butylation, phenol co-adsorbs with TBA through formation of a hydrogen bond between the H atom in hydroxyl and the zeolite framework O atom (H_{phenol}–$O_{zeolite}$ is 2.54 Å) in addition to the σ–π interaction between phenol and TBA. However, in 4-tert-butylation, phenol co-adsorbs with TBA only by σ–π interaction. Therefore, the co-adsorbed reactant **Co2_Ads** in 2-tert-butylation is more stable. The activation barriers for 2- and 4-tert-butylation are 29.0 and 21.4 kcal mol^{-1}, respectively. 4-Tert-butylation, with a lower E_{act}, is kinetically favored over 2-tert-butylation. Formation of adsorbed 2-TBP from the co-adsorbed state is exothermic by 6.1 kcal mol^{-1}, whereas it is 16.6 kcal mol^{-1} exothermic for adsorbed 4-TBP formation.

3.3. Comparison of the stepwise and the concerted paths

The above results can be used to examine tert-butylation of phenol with TBA over Al-H-β zeolite through either the stepwise or the concerted mechanism. Table 4 lists the major comparison items between these two reaction paths. Based on the definition in Murdoch's procedure [39], the apparent activation barrier ($E_{app\text{-}act}$) can be approximated as 47.4 kcal mol^{-1} for 2-TBP formation and 46.2 kcal mol^{-1} for 4-TBP formation in the stepwise path, whereas it is 33.1 kcal mol^{-1} for 2-tert-butylation and 26.6 kcal mol^{-1} for 4-tert-butylation in the concerted path. The 14.3 and 19.6 kcal mol^{-1} differences in $E_{app\text{-}act}$ for 2-TBP and 4-TBP formation between these two reaction paths indicate that the concerted mechanism is preferred for phenol tert-butylation. The $E_{app\text{-}act}$ difference between 2- and 4-tert-butylation is more obvious in the concerted path

Table 4
Major comparison items between the stepwise and concerted mechanisms[a].

Comparison item	Stepwise path		Concerted path	
	2-Tert-butylation	4-Tert-butylation	2-Tert-butylation	4-Tert-butylation
$E_{app\text{-}act}$	47.4	46.2	33.1	26.6
TS stability[b]	17.4	16.2	−15.4	−18.0
TS structure	TS_2-TBP	TS_4-TBP	TS_2-TBP	TS_4-TBP
H_{phenol} donated $O_{zeolite}$	O_1		O_2	
H_{phenol}–$O_{zeolite}$	1.65	1.61	1.36	1.36
C_{phenol}–$O_{zeolite}$	3.01	2.95	2.83	2.82
Water	Desorbed prior to tert-butylation		Retained throughout the reaction	

[a] Energy unit is in kcal mol^{-1}, and bond distances are in Angstroms.
[b] The energy of separated TBA, Al-H-β plus separated phenol is used as the reference point.

Table 5
Comparison energetics of tert-butylation of phenol with TBA in both reaction paths over Ga-H-β and Al-H-β zeolites[a].

Reaction path	Key step	Ga-H-β	Al-H-β
Stepwise	E_{ads} of TBA	−27.0	−30.0
	E_{act} on formation of *t*-butyl carbenium ion product	33.3	30.6
	$E_{app\text{-}act}$ on 2-tert-butylation	53.1	47.4
	$E_{app\text{-}act}$ on 4-tert-butylation	52.8	46.2
Concerted	$E_{co\text{-}ads}$ of TBA with phenol[b]	−41.0, −35.1	−44.4, −39.4
	$E_{app\text{-}act}$ on 2-tert-butylation	40.5	33.1
	$E_{app\text{-}act}$ on 4-tert-butylation	36.2	26.6

[a] Energy unit is in kcal mol^{-1}.
[b] Data in front belongs to 2-tert-butylation.

(6.5 kcal mol^{-1}) than in the stepwise path (1.2 kcal mol^{-1}), where 4-tert-butylation proceeds faster.

Though the apparent activation barrier differences are less than 20 kcal mol^{-1} between the concerted and stepwise paths, the stability of the transition states between these two reaction paths show larger differences (32.8 and 34.2 kcal mol^{-1} for **TS_2-TBP** and **TS_4-TBP**, respectively). To explain the big difference in transition state stability, we examine the molecular structure of each transition state. The transition state configurations in the stepwise path shown in Fig. 4(c) and (d) and in the concerted path shown in Fig. 6(c) and (d) all involve the formation of a C_1–C_2 bond, complete dissociation of the C_1–H_1 bond, and partial creation of a H_1–$O_{zeolite}$ bond. However, the phenol tert-butylation intermediate donates a proton to different zeolite O atoms between these two mechanisms. In the stepwise path, the H_{phenol} goes back to O_1, whereas the H_{phenol} donates to O_2 in the concerted path. Therefore, the differences in the corresponding H_{phenol}–$O_{zeolite}$ interaction and the C_{phenol}–$O_{zeolite}$ distance likely impact the transition state stability of these two paths. As shown in Table 4, the transition states created in the concerted mechanism should be more stable than those in the stepwise path as reflected by a stronger hydrogen bond between the H_{phenol} and $O_{zeolite}$, as well as a closer distance of the C_{phenol}–$O_{zeolite}$. However, the choice of which O atom the proton begins the reaction bound to was arbitrary, and presumably the next catalytic cycle would begin with the proton in its final position. Therefore, though these differences contribute to the reported transition state stability differences, they are not significant in differentiating whether the stepwise or concerted paths would be preferred.

A significant difference dictating the relative transition state stability between the stepwise and concerted paths is the inclusion of the water molecule in the concerted path. In the stepwise path, we did not include a co-adsorbed water molecule during the alkylation reaction, and therefore we define the "stepwise mechanism" to require water desorption prior to tert-butylation. If water is retained near to the active center during the tert-butylation step, the "concerted" transition state would be accessible within the stepwise mechanism with the water molecule in the same position. We note again that the water molecule is completely formed at the transition state for the concerted path. Therefore, the rate of a "water-assisted stepwise mechanism" would be identical to the concerted path, and the only meaningful kinetic differentiation between the stepwise and concerted paths is the requirement that water desorption precede alkylation in the stepwise mechanism. The calculated desorption energy of water is 12.7 kcal mol^{-1} in the stepwise path, thus the transition states created in the concerted path including water adsorption interaction can gain extra stability than those produced in the stepwise path without water.

3.4. Impact of the acid site strength of H-β

Experimental studies [9–11] indicate that acid site strength impacts catalytic activity for this reaction. We introduced Ga-H-β as the acid catalyst to compare with Al-H-β to gain insight into the influence of acid site strength. This substitution allows for directly accessing the impact of acid site strength with minimal change in site structure. The proton affinity [PA, Eq. (1)] and adsorption energy of basic probe molecules [$\Delta E_{(ads)}$, Eq. (2)] are two common methods to characterize the acid site strength of zeolites in theoretical studies [40–49]. We calculated the PA of beta zeolites and adsorption energy of an NH_3 molecule over Ga-H-β and Al-H-β. The PA of Ga-H-β is −294.6 kcal mol^{-1}, which is 4.9 kcal mol^{-1} more negative than that of Al-H-β. A more negative PA indicates a stronger interaction of ZeO^- with the proton, thus a weaker acid site of the corresponding ZeOH. The acid site strength of Al-H-β is therefore stronger than Ga-H-β, which is in agreement with a previous study from Wang's group [50]. NH_3 adsorption energy results show that adsorption on Al-H-β is 3.1 kcal mol^{-1} more exothermic than on Ga-H-β, also indicative of the Al form being a stronger acid site.

Tert-butylation of phenol with TBA over Ga-H-β was investigated and compared with Al-H-β. The comparison results of key steps in both reaction paths are given in Table 5. The adsorption energies (−27.0 kcal mol^{-1} for TBA adsorption, −41.0 and −35.1 kcal mol^{-1} for TBA with phenol co-adsorption) over Ga-H-β are weaker than those over Al-H-β (−30.0, −44.4 and −39.4 kcal mol^{-1}, respectively). Over the less acidic Ga-H-β, the proton is more tightly bound and therefore less available to form a hydrogen bond between the acid site and hydroxyl group of TBA. The E_{act} for tert-butyl carbenium ion formation in the stepwise mechanism with Ga-H-β increases due to the weaker acid site strength. The $E_{app\text{-}act}$ for tert-butylation steps are increased for both 2- and 4-tert-butylation using Ga-H-β. However, the $\Delta E_{app\text{-}act}$ between 2- and 4-tert-butylation becomes smaller, indicating the selectivity to 4-TBP formation is decreased. By adjusting acid site strength of the zeolite, the catalytic activity and product selectivity can be tuned. By comparison of the calculation results using these two acidic H-β zeolites, we can conclude that with decreasing acid site strength, the tert-butylation rate and the product selectivity toward 4-TBP are decreased.

4. Conclusions

The proposed stepwise and concerted mechanisms for tert-butylation of phenol with tert-butyl alcohol over H-β zeolite have been investigated theoretically using the two-layered ONIOM (B3LYP/6-31G(d,p):UFF) approach. Computational results reveal that tert-butylation of phenol preferentially occurs through a concerted path involving co-adsorption and reaction of tert-butyl alcohol and phenol without prior dehydration of tert-butyl alcohol, rather than through a stepwise path via dehydration to form a carbenium ion as the first step followed by tert-butyl cation attack on the 2- and 4-position on phenol. The kinetic difference between 2- and 4-tert-butylation is more apparent in the concerted mechanism, where 4-tert-butylation proceeds faster. Decreasing the acid site strength increases the activation barriers, thus lower-

ing the reaction rate, and also decreases the selectivity to 4-TBP. The present study on an industrially important and well-known reaction demonstrates that a detailed computational study can uncover a kinetically more favored reaction pathway (the concerted mechanism) which is distinctly different from the commonly envisioned stepwise pathway.

Acknowledgements

This work was financially supported by the program for New Century Excellent Talent in University (NCET-04-0268) and the Plan 111 Project of the Ministry of Education of China. The authors also thank the Pennsylvania State University for partial financial support for X.W. Nie as a part of the collaborative research in the ongoing PSU-DUT Clean Energy Research Center efforts.

Appendix A. Supplementary data

Supplementary data associated with this article can be found, in the online version, at doi:10.1016/j.cattod.2010.11.070.

The imaginary frequency values for each transition state created, the Cartesian coordinates for all stationary points included in both the reaction mechanisms with Al-H-β and Ga-H-β, and two kinds of phenol adsorption models together with the corresponding adsorption energies over Al-H-β zeolite. These materials are available free of charge via the Internet at http://www.sciencedirect.com.

References

[1] R.A. van Santen, G.J. Kramer, Chem. Rev. 95 (1995) 637–660.
[2] F. Zhou, X. Li, A.J. Wang, L.Y. Wang, X.D. Yang, Y.K. Hu, Catal. Today 150 (2010) 218–223.
[3] L. Lang, X.F. Liu, M.L. Hu, B.Q. Zhang, Chemcatchem 1 (2009) 472–478.
[4] F. Jin, Y.D. Li, Catal. Lett. 131 (2009) 545–551.
[5] F. Neatu, S. Coman, V.I. Parvulescu, G. Poncelet, D. De Vos, P. Jacobs, Top. Catal. 52 (2009) 1292–1300.
[6] T. Danuthai, S. Jongpatiwut, T. Rirksomboon, S. Osuwan, D.E. Resasco, Appl. Catal. A: Gen. 361 (2009) 99–105.
[7] R. Gonzalez-Olmos, U. Roland, H. Toufar, F.D. Kopinke, A. Georgi, Appl. Catal. B: Environ. 89 (2009) 356–364.
[8] F. Yaripour, A. Mollavali, S.M. Jam, H. Atashi, Energy Fuels 23 (2009) 1896–1900.
[9] K. Zhang, C. Huang, H. Zhang, S. Xiang, S. Liu, D. Xu, H. Li, Appl. Catal. A: Gen. 166 (1998) 89–95.
[10] A. Sakthivel, S.K. Badamali, P. Selvam, Micropor. Mesopor. Mater. 39 (2000) 457–463.
[11] K. Song, J.Q. Guan, S.J. Wu, Y. Yang, B. Liu, Q.B. Kan, Catal. Lett. 126 (2008) 333–340.
[12] S.G. Hegde, R. Kumar, R.N. Bhat, P. Ratnasamy, Zeolites 9 (1989) 231–237.
[13] A. Vinu, B.M. Devassy, S.B. Halligudi, W. Bohlmann, M. Hartmann, Appl. Catal. A: Gen. 281 (2005) 207–213.
[14] P.E. Sinclair, A. de Vries, P. Sherwood, C.R.A. Catlow, R.A. van Santen, J. Chem. Soc. Faraday Trans. 94 (1998) 3401–3408.
[15] M. Brandle, J. Sauer, J. Am. Chem. Soc. 120 (1998) 1556–1570.
[16] L.A. Clark, M. Sierka, J. Sauer, J. Am. Chem. Soc. 125 (2003) 2136–2141.
[17] S. Kasuriya, S. Namuangruk, P. Treesukol, M. Tirtowidjojo, J. Limtrakul, J. Catal. 219 (2003) 320–328.
[18] S. Namuangruk, P. Pantu, J. Limtrakul, J. Catal. 225 (2004) 523–530.
[19] P. Pantu, S. Pabchanda, J. Limtrakul, Chemphyschem 5 (2004) 1901–1906.
[20] S. Namuangruk, P. Khongpracha, P. Pantu, J. Limtrakul, J. Phys. Chem. B 110 (2006) 25950–25957.
[21] S. Pabchanda, P. Pantu, J. Limtrakul, J. Mol. Catal. A: Chem. 239 (2005) 103–110.
[22] J.M. Newsam, M.M.J. Treacy, W.T. Koetsier, C.B.D. Gruyter, Proc. R. Soc. Lond. A Mater. 420 (1988) 375–405.
[23] A.H. de Vries, P. Sherwood, S.J. Collins, A.M. Rigby, M. Rigutto, G.J. Kramer, J. Phys. Chem. B 103 (1999) 6133–6141.
[24] R. Hajjar, Y. Millot, P.P. Man, M. Che, S. Dzwigaj, J. Phys. Chem. C 112 (2008) 20167–20175.
[25] H. Fujita, T. Kanougi, T. Atoguchi, Appl. Catal. A: Gen. 313 (2006) 160–166.
[26] A.K. Rappe, C.J. Casewit, K.S. Colwell, W.A. Goddard, W.M. Skiff, J. Am. Chem. Soc. 114 (1992) 10024–10035.
[27] M.J. Frisch, G.W. Trucks, H.B. Schlegel, G.E. Scuseria, M.A. Robb, J.R. Cheeseman, J.A. Montgomery, J.T. Vreven, K.N. Kudin, J.C. Burant, J.M. Millam, S.S. Iyengar, J. Tomasi, V. Barone, B. Mennucci, M. Cossi, G. Scalmani, N. Rega, G.A. Petersson, H. Nakatsuji, M. Hada, M. Ehara, K. Toyota, R. Fukuda, J. Hasegawa, M. Ishida, T. Nakajima, Y. Honda, O. Kitao, H. Nakai, M. Klene, X. Li, J.E. Knox, H.P. Hratchian, J.B. Cross, C. Adamo, J. Jaramillo, R. Gomperts, R.E. Stratmann, O. Yazyev, A.J. Austin, R. Cammi, C. Pomelli, J.W. Ochterski, P.Y. Ayala, K. Morokuma, G.A. Voth, P. Salvador, J.J. Dannenberg, V.G. Zakrzewski, S. Dapprich, A.D. Daniels, M.C. Strain, O. Farkas, D.K. Malick, A.D. Rabuck, K. Raghavachari, J.B. Foresman, J.V. Ortiz, Q. Cui, A.G. Baboul, S. Clifford, J. Cioslowski, B.B. Stefanov, G. Liu, A. Liashenko, P. Piskorz, I. Komaromi, R.L. Martin, D.J. Fox, T. Keith, M.A. Al-Laham, C.Y. Peng, A. Nanayakkara, M. Challacombe, P.M.W. Gill, B. Johnson, W. Chen, M.W. Wong, C. Gonzalez, J.A. Pople, Gaussian 03 (Revision E.01), Gaussian, Inc., Pittsburgh, PA, 2003.
[28] X.W. Nie, X. Liu, C.S. Song, X.W. Guo, Chin. J. Catal. 30 (2009) 453–458.
[29] B. Jansang, T. Nanok, J. Limtrakul, J. Phys. Chem. C 112 (2008) 540–547.
[30] M.J. Janik, J. Macht, E. Iglesia, M. Neurock, J. Phys. Chem. C 113 (2009) 1872–1885.
[31] J.N. Kondo, K. Ito, E. Yoda, F. Wakabayashi, K. Domen, J. Phys. Chem. B 109 (2005) 10969–10972.
[32] J. Bedia, R. Ruiz-Rosas, J. Rodriguez-Mirasol, T. Cordero, J. Catal. 271 (2010) 33–42.
[33] Y.K. Kim, R. Rousseau, B.D. Kay, J.M. White, Z. Dohnalek, J. Am. Chem. Soc. 130 (2008) 5059–5061.
[34] C.C. Lee, R.J. Gorte, W.E. Farneth, J. Phys. Chem. B 101 (1997) 3811–3817.
[35] U. Messow, K. Quitzsch, H. Herden, Zeolites 4 (1984) 255–258.
[36] C. Kumsapaya, K. Bobuatong, P. Khongpracha, Y. Tantirungrotechai, J. Limtrakul, J. Phys. Chem. C 113 (2009) 16128–16137.
[37] T. Sasaki, M. Tada, Y. Iwasawa, Top. Catal. 52 (2009) 880–887.
[38] A.A. Shubin, C.R.A. Catlow, J.M. Thomas, K.I. Zamaraev, Proc. R. Soc. Lond. A 446 (1994) 411–427.
[39] J.R. Murdoch, J. Chem. Educ. 58 (1981) 32–36.
[40] C. Busco, A. Barbaglia, M. Broyer, V. Bolis, G.M. Foddanu, P. Ugliengo, Thermochim. Acta 418 (2004) 3–9.
[41] D.H. Zhou, Y. Bao, M.M. Yang, N. He, G. Yang, J. Mol. Catal. A: Chem. 244 (2006) 11–19.
[42] A.M. Zheng, L. Chen, J. Yang, M.J. Zhang, Y.C. Su, Y. Yue, C.H. Ye, F. Deng, J. Phys. Chem. B 109 (2005) 24273–24279.
[43] N. Jiang, S.P. Yuan, J.G. Wang, H.J. Jiao, Z.F. Qin, Y.W. Li, J. Mol. Catal. A: Chem. 220 (2004) 221–228.
[44] A. Chatterjee, A.K. Chandra, J. Mol. Catal. A: Chem. 119 (1997) 51–56.
[45] Y.L. Wang, Z.G. Lei, B.H. Chen, Q.H. Guo, N. Liu, Appl. Surf. Sci. 256 (2010) 4042–4047.
[46] S.P. Yuan, J.U. Wang, Y.B. Duan, Y.W. Li, H.J. Jiao, J. Mol. Catal. A: Chem. 256 (2006) 130–137.
[47] N. Injan, N. Pannorad, M. Probst, J. Limtrakul, Int. J. Quantum Chem. 105 (2005) 898–905.
[48] H.V. Brand, A. Redondo, P.J. Hay, J. Mol. Catal. A: Chem. 121 (1997) 45–62.
[49] J.B. Nicholas, Top. Catal. 4 (1997) 157–171.
[50] S.P. Yuan, J.G. Wang, Y.W. Li, S.Y. Peng, Acta Phys. Chim. Sin. 17 (2001) 811–816.